Spin-adapted open-shell time-dependent density functional theory. III. An even better and simpler formulation

Zhendong Li, and Wenjian Liu

Citation: The Journal of Chemical Physics **135**, 194106 (2011); doi: 10.1063/1.3660688
View online: https://doi.org/10.1063/1.3660688
View Table of Contents: http://aip.scitation.org/toc/jcp/135/19
Published by the American Institute of Physics

Spin-adapted open-shell time-dependent density functional theory. III. An even better and simpler formulation

Zhendong Li and Wenjian Liu[a)]
Beijing National Laboratory for Molecular Sciences, Institute of Theoretical and Computational Chemistry, State Key Laboratory of Rare Earth Materials Chemistry and Applications, College of Chemistry and Molecular Engineering, and Center for Computational Science and Engineering, Peking University, Beijing 100871, People's Republic of China

(Received 22 September 2011; accepted 25 October 2011; published online 18 November 2011)

The recently proposed spin-adapted time-dependent density functional theory (S-TD-DFT) [Z. Li and W. Liu, J. Chem. Phys. **133**, 064106 (2010)] resolves the spin-contamination problem in describing singly excited states of high spin open-shell systems. It is an extension of the standard restricted open-shell Kohn-Sham-based TD-DFT which can only access those excited states due to singlet-coupled single excitations. It is also far superior over the unrestricted Kohn-Sham-based TD-DFT (U-TD-DFT) which suffers from severe spin contamination for those excited states due to triplet-coupled single excitations. Nonetheless, the accuracy of S-TD-DFT for high spin open-shell systems is still inferior to TD-DFT for well-behaved closed-shell systems. The reason can be traced back to the violation of the spin degeneracy conditions (SDC) by approximate exchange-correlation (XC) functionals. Noticing that spin-adapted random phase approximation (S-RPA) can indeed maintain the SDC by virtue of the Wigner-Eckart theorem, a hybrid ansatz combining the good of S-TD-DFT and S-RPA can immediately be envisaged. The resulting formalism, dubbed as X-TD-DFT, is free of spin contamination and can also be viewed as a S-RPA correction to the XC kernel of U-TD-DFT. Compared with S-TD-DFT, X-TD-DFT leads to much improved results for the low-lying excited states of, e.g., N_2^+, yet with much reduced computational cost. Therefore, X-TD-DFT can be recommended for routine calculations of excited states of high spin open-shell systems. [doi:10.1063/1.3660688]

I. INTRODUCTION

Theoretical investigations of excited states of molecular systems are of vast importance for the understanding of luminescence processes and excited state chemistry. In this context, equation-of-motion coupled-cluster theory with singles and doubles (EOM-CCSD) (Refs. 1 and 2) can usually provide benchmarks for closed-shell molecules. Time-dependent density functional linear response theory[3–5] (TD-DFT) is also very useful due to its efficiency and reliability. However, both sets of methods face great difficulties even for open-shell systems that can well be represented by a single determinant. This can be illustrated by a prototypical three-electron-three-level doublet model (cf. Fig. 1). Taking the high spin component $\Psi_0 = |i\bar{i}t\rangle$ as the reference, the first two (i.e., $\Psi_i^a = |a\bar{i}t\rangle$ and $\Psi_{\bar{i}}^{\bar{a}} = |i\bar{a}t\rangle$) and the third (i.e., $\Psi_{\bar{i}t}^{\bar{i}a} = |i\bar{i}a\rangle = a_{\bar{i}}^\dagger a_{\bar{i}} a_a^\dagger a_t |i\bar{i}t\rangle$) determinants arise from spin-conserving single and double excitations, respectively. As a result, the determinant $\Psi_{\bar{i}t}^{\bar{i}a}$ cannot be treated by EOM-CCSD in a balanced manner relative to the other two, implying that at least triple excitations are required for a reliable estimate of the corresponding excitation energy.[6,7] The problem encountered in TD-DFT is even more severe, since the determinant $\Psi_{\bar{i}t}^{\bar{i}a}$ is excluded by the adiabatic approximation that allows only single excitations. Consequently, adiabatic TD-DFT will give rise to a pure doublet state arising from the singlet-coupled single excitation (SCSE),

$$S_{ai}^\dagger(0,0)|\Psi_0\rangle = \frac{1}{\sqrt{2}}\left(\Psi_i^a + \Psi_{\bar{i}}^{\bar{a}}\right), \tag{1}$$

as well as a mixed-spin state arising from the triplet-coupled single excitation (TCSE),

$$T_{ai}^\dagger(0,0)|\Psi_0\rangle = \frac{1}{\sqrt{2}}\left(\Psi_i^a - \Psi_{\bar{i}}^{\bar{a}}\right). \tag{2}$$

More precisely, the latter is a 1:2 mixture of a doublet $|D_2\rangle$ and a quartet $|Q_1\rangle$, viz.,

$$|D_2\rangle = \frac{1}{\sqrt{6}}\left(-\Psi_i^a + \Psi_{\bar{i}}^{\bar{a}} + 2\Psi_{\bar{i}t}^{\bar{i}a}\right), \tag{3}$$

$$|Q_1\rangle = \frac{1}{\sqrt{3}}\left(\Psi_i^a - \Psi_{\bar{i}}^{\bar{a}} + \Psi_{\bar{i}t}^{\bar{i}a}\right). \tag{4}$$

It is generally true that, for a high spin open-shell reference, the TSCE from closed- to vacant-shell orbitals lead always to spin-contaminated states.[8,9] A more detailed analysis of the spin structure of singly excited states can be found from Table I in Ref. 10.

This problem is resolved only recently by the spin-adapted TD-DFT (S-TD-DFT).[10,11] The underlying tensor-based formulation takes all the components of a spin multiplet S_i as the reference and is conceptually different from the one[12] that takes only one component of the spin multiplet

a)Author to whom correspondence should be addressed. Electronic mail: liuwjbdf@gmail.com.

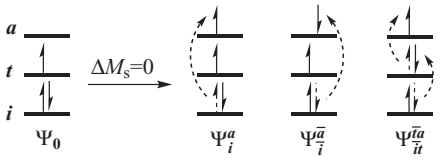

FIG. 1. Three-level model for closed- to vacant-shell transitions.

S_i as the reference. The former invokes only spin-conserving ($\Delta M_s = 0$) and spin-flip ($\Delta M_s = \pm 1$) single excitation operators, whereas the latter has to introduce some generalized orbital excitation operators. What is particularly interesting is that the final S-TD-DFT equations for different spin states ($S_f = S_i - 1$, S_i, or $S_i + 1$) involve explicitly only the high spin component of the spin multiplet S_i. In other words, the contributions of those higher-rank excitations, as viewed by taking only one component of the multiplet as the reference, are fixed by spin symmetry and can be folded into the corresponding Racah and Clebsch-Gordan coefficients, such that they even do not enter into the operator matrix elements.[11] The difference between the matrix elements for the excited states of spin $S_i - 1$, S_i, and $S_i + 1$ resides only in the Racah coefficients, such that the excited states of different spin can be obtained in one shot once the (single excitation) operator matrix elements over the high spin reference are available. In this way, S-TD-DFT provides a balanced description of all the excited states shown in Fig. 1 even under the adiabatic approximation, since the determinant $\Psi_{\bar{i}t}^{\bar{i}a}$ now becomes a flip-up single excitation from the $M_s = -1/2$ component of the doublet state, viz., $\Psi_{\bar{i}t}^{\bar{i}a} = |i\bar{t}a\rangle = -a_a^\dagger a_{\bar{i}}|i\bar{i}\bar{t}\rangle$. It has been demonstrated[10] that, for the low-lying excited states of N_2^+, S-TD-DFT can reduce the errors of U-TD-DFT (unrestricted Kohn-Sham-based TD-DFT) by ~1 eV for those heavily spin-contaminated states. However, the overall accuracy of S-TD-DFT for open-shell systems is still inferior to that (typically 0.2–0.3 eV (Ref. 13)) of TD-DFT for singlet excited states of well-behaved closed-shell systems.

At first, one might expect that the accuracy of S-TD-DFT may steadily be improved by climbing up the Jacob ladder of exchange-correlation (XC) functionals.[14] Unfortunately, this is not necessarily the case. In particular, hybrid functionals may perform very poorly due to the Hartree-Fock (HF) instability problem that is often encountered in open-shell systems. Instead, it is the spin degeneracy conditions (SDC, vide post) ensuring the degeneracy of different components of an excited-state multiplet that play the first important role. Although the SDC are fulfilled automatically in the spin-adapted random phase approximation (S-RPA) (Ref. 11) by virtue of the Wigner-Eckart theorem, they are violated by all the currently available approximate XC functionals. This observation leads immediately to a reformulation of S-TD-DFT so as to explicitly incorporate the SDC. The resulting formalism, to be dubbed as X-TD-DFT, becomes more accurate and even simpler than the parent S-TD-DFT. It combines the good of S-TD-DFT and S-RPA and can also be viewed as a S-RPA correction to the XC kernel of U-TD-DFT. The new formulation will be detailed in Sec. II, where the following convention for labeling the molecular orbitals is to be employed: $\{i, j, k, l, \ldots\}$ for doubly occupied orbitals (closed shell part, C), $\{t, u, v, w, \ldots\}$ for singly occupied orbitals and their time-reversed partners (open shell part, O), $\{a, b, c, d, \ldots\}$ for virtual orbitals (vacant shell part, V), and $\{p, q, r, s, \ldots\}$ for unspecified orbitals. They are all assumed to be real valued since only spin-free Hamiltonians, nonrelativistic or scalar relativistic, are under concern here. Greek indices are used to denote electron spin.

II. THEORY

A. S-TD-DFT

U-TD-DFT amounts to solving the following pseudo-eigenvalue problem:

$$\begin{bmatrix} \mathbf{A} & \mathbf{B} \\ \mathbf{B} & \mathbf{A} \end{bmatrix} \begin{bmatrix} \mathbf{X} \\ \mathbf{Y} \end{bmatrix} = \omega \begin{bmatrix} \mathbf{I} & \mathbf{0} \\ \mathbf{0} & -\mathbf{I} \end{bmatrix} \begin{bmatrix} \mathbf{X} \\ \mathbf{Y} \end{bmatrix}, \tag{5}$$

$$[\mathbf{A}^{\sigma\tau,\sigma'\tau'}]_{pq,rs} = \delta_{\sigma\sigma'}\delta_{\tau\tau'}\left(\delta_{qs}F_{pr}^{\sigma} - \delta_{pr}F_{sq}^{\tau}\right) + [K^{\sigma\tau,\sigma'\tau'}]_{pq,rs}, \tag{6}$$

$$[\mathbf{B}^{\sigma\tau,\sigma'\tau'}]_{pq,rs} = [K^{\sigma\tau,\tau'\sigma'}]_{pq,sr}, \tag{7}$$

where F^σ is the unrestricted KS (UKS) matrix for spin σ and the adiabatic coupling matrix is defined as

$$[K^{\sigma\tau,\sigma'\tau'}]_{pq,rs} = (p_\sigma q_\tau|s_{\tau'}r_{\sigma'}) + \left[K_{XC}^{\sigma\tau,\sigma'\tau'}\right]_{pq,rs}. \tag{8}$$

The Mulliken notation has been employed for the integrals. The second term in Eq. (8) represent the matrix elements of the XC kernel $f_{XC}^{\sigma\tau,\sigma'\tau'}$, whose explicit form depends on the chosen XC functional.

The working equation of S-TD-DFT (Ref. 10 and 11) for spin-allowed excitations can also be cast into form (5), with the **A** and **B** matrices given in Table I. For high spin open-shell systems considered here, the spin-conserving excitations can, in the spin-tensor basis (cf. Eqs. (1) and (2)), be classified into four types, i.e., CO(0), OV(0), CV(0), and CV(1). Here, the symbol CO(Γ) represents a transition from a closed- to an open-shell orbital (Γ = 0 for SCSE and Γ = 1 for TCSE). Other symbols are defined similarly. For the first three kinds of excitations, the **A** and **B** matrices of S-TD-DFT are identical with those of U-TD-DFT, if the spin-tensor basis instead of the spin-orbital basis is also employed in the latter. However, for the CV(1) type of excitations, the **A** matrix of S-TD-DFT differs from that of U-TD-DFT by

$$[\Delta\mathbf{A}]_{ai,bj} = \frac{1}{S_i}\left(\delta_{ij}F_{ab}^S + \delta_{ab}F_{ji}^S\right), \quad F_{pq}^S = \frac{1}{2}\left(F_{pq}^\beta - F_{pq}^\alpha\right), \tag{9}$$

provided that the differences between the UKS and restricted open-shell KS (ROKS) orbitals can be neglected. This correction term stems obviously from spin polarizations in the open-shell ground state. Only in the limit of an infinite number of open-shell electrons (i.e., $S_i \to \infty$), the correction $\Delta\mathbf{A}$ vanishes and S-TD-DFT and U-TD-DFT then become identical.

TABLE I. Independent matrix elements of **A** and **B** in S-TD-DFT. The $K^{\sigma\tau,\sigma'\tau'}$ matrices are defined in Eq. (8). S_i: total spin of the reference.

Blocks	Matrix elements[a]
CV(0)-CV(0)	$[\mathbf{A}]_{ai,bj} = \delta_{ij}(\frac{F^{\alpha}_{ab}+F^{\beta}_{ab}}{2}) - \delta_{ab}(\frac{F^{\alpha}_{ji}+F^{\beta}_{ji}}{2}) + [K^S]_{ai,bj}$
CV(0)-CO(0)	$[\mathbf{A}]_{ai,vj} = \frac{1}{\sqrt{2}}(\delta_{ij}F^{\beta}_{av} + [K^{\alpha\alpha,\beta\beta}]_{ai,vj} + [K^{\beta\beta,\beta\beta}]_{ai,vj})$
CV(0)-OV(0)	$[\mathbf{A}]_{ai,bv} = \frac{1}{\sqrt{2}}(-\delta_{ab}F^{\alpha}_{vi} + [K^{\alpha\alpha,\alpha\alpha}]_{ai,bv} + [K^{\beta\beta,\alpha\alpha}]_{ai,bv})$
CO(0)-CO(0)	$[\mathbf{A}]_{ui,vj} = \delta_{ij}F^{\beta}_{uv} - \delta_{uv}F^{\beta}_{ji} + [K^{\beta\beta,\beta\beta}]_{ui,vj}$
CO(0)-OV(0)	$[\mathbf{A}]_{ui,bv} = [K^{\beta\beta,\alpha\alpha}]_{ui,bv}$
OV(0)-OV(0)	$[\mathbf{A}]_{au,bv} = \delta_{uv}F^{\alpha}_{ab} - \delta_{ab}F^{\alpha}_{vu} + [K^{\alpha\alpha,\alpha\alpha}]_{au,bv}$
CV(0)-CV(1)	$[\mathbf{A}]_{ai,bj} = -\sqrt{\frac{S_i+1}{S_i}}(\delta_{ij}(\frac{F^{\alpha}_{ab}-F^{\beta}_{ab}}{2}) - \delta_{ab}(\frac{F^{\alpha}_{ji}-F^{\beta}_{ji}}{2}) + [K^P]_{ai,bj})$
CO(0)-CV(1)	$[\mathbf{A}]_{ui,bj} = -\sqrt{\frac{S_i+1}{S_i}}\frac{1}{\sqrt{2}}(-\delta_{ij}F^{\beta}_{ub} + [K^{\beta\beta,\alpha\alpha}]_{ui,bj} - [K^{\beta\beta,\beta\beta}]_{ui,bj})$
OV(0)-CV(1)	$[\mathbf{A}]_{au,bj} = -\sqrt{\frac{S_i+1}{S_i}}\frac{1}{\sqrt{2}}(-\delta_{ab}F^{\alpha}_{ju} + [K^{\alpha\alpha,\alpha\alpha}]_{au,bj} - [K^{\alpha\alpha,\beta\beta}]_{au,bj})$
CV(1)-CV(1)	$[\mathbf{A}]_{ai,bj} = \delta_{ij}[\frac{1}{2}(1-\frac{1}{S_i})F^{\alpha}_{ab} + \frac{1}{2}(1+\frac{1}{S_i})F^{\beta}_{ab}]$ $-\delta_{ab}[\frac{1}{2}(1+\frac{1}{S_i})F^{\alpha}_{ji} + \frac{1}{2}(1-\frac{1}{S_i})F^{\beta}_{ji}] + [K^T]_{ai,bj}$
CV(0)-CV(0)	$[\mathbf{B}]_{ai,bj} = [K^S]_{ai,jb}$
CV(0)-CO(0)	$[\mathbf{B}]_{ai,vj} = \frac{1}{\sqrt{2}}([K^{\alpha\alpha,\beta\beta}]_{ai,jv} + [K^{\beta\beta,\beta\beta}]_{ai,jv})$
CV(0)-OV(0)	$[\mathbf{B}]_{ai,bv} = \frac{1}{\sqrt{2}}([K^{\alpha\alpha,\alpha\alpha}]_{ai,vb} + [K^{\beta\beta,\alpha\alpha}]_{ai,vb})$
CO(0)-CO(0)	$[\mathbf{B}]_{ui,vj} = [K^{\beta\beta,\beta\beta}]_{ui,jv}$
CO(0)-OV(0)	$[\mathbf{B}]_{ui,bv} = \delta_{uv}F^{\beta}_{bi} + [K^{\beta\beta,\alpha\alpha}]_{ui,vb}$
OV(0)-OV(0)	$[\mathbf{B}]_{au,bv} = [K^{\alpha\alpha,\alpha\alpha}]_{au,vb}$
CV(0)-CV(1)	$[\mathbf{B}]_{ai,bj} = -\sqrt{\frac{S_i+1}{S_i}}[K^P]_{ai,jb}$
CO(0)-CV(1)	$[\mathbf{B}]_{ui,bj} = -\sqrt{\frac{S_i+1}{S_i}}\frac{1}{\sqrt{2}}([K^{\beta\beta,\alpha\alpha}]_{ui,jb} - [K^{\beta\beta,\beta\beta}]_{ui,jb})$
OV(0)-CV(1)	$[\mathbf{B}]_{au,bj} = -\sqrt{\frac{S_i+1}{S_i}}\frac{1}{\sqrt{2}}([K^{\alpha\alpha,\alpha\alpha}]_{au,jb} - [K^{\alpha\alpha,\beta\beta}]_{au,jb})$
CV(1)-CV(1)	$[\mathbf{B}]_{ai,bj} = [K^T]_{ai,jb}$

[a] $K^S = \frac{1}{2}(K^{\alpha\alpha,\alpha\alpha} + K^{\alpha\alpha,\beta\beta} + K^{\beta\beta,\alpha\alpha} + K^{\beta\beta,\beta\beta})$,
$K^P = \frac{1}{2}(K^{\alpha\alpha,\alpha\alpha} - K^{\alpha\alpha,\beta\beta} + K^{\beta\beta,\alpha\alpha} - K^{\beta\beta,\beta\beta})$,
$K^T = \frac{1}{2}(K^{\alpha\alpha,\alpha\alpha} - K^{\alpha\alpha,\beta\beta} - K^{\beta\beta,\alpha\alpha} + K^{\beta\beta,\beta\beta})$.

Otherwise, the diagonal elements of $\Delta\mathbf{A}$ are always positive-valued, such that the U-TD-DFT excitation energies for the CV(1) type of excitations are always blueshifted by S-TD-DFT in the right direction. Yet, the overall accuracy of S-TD-DFT for high spin open-shell systems is still inferior to that of TD-DFT for closed-shell systems.[10] To find out the possible source of remaining errors, we shall take a close scrutiny of the formulation of S-TD-DFT.

B. The spin degeneracy conditions

The particular S-TD-DFT is born of the S-RPA, which can generally be expressed as a generalized eigenvalue equation,[11]

$$\mathbf{M}_{S_f}\mathbf{X}_\lambda = \omega_\lambda \mathbf{N}_{S_f}\mathbf{X}_\lambda, \tag{10}$$

where both $\mathbf{M}_{S_f}$ and $\mathbf{N}_{S_f}$ depend on the excited state spin S_f but not on the spin-projection M_f ($= -S_f, -S_f+1, \ldots, S_f$). This important feature results directly from the Wigner-Eckart theorem and is the key for ensuring the precise degeneracy of different components of an excited state multiplet. The S-RPA is then "translated" to S-TD-DFT, simply by replacing the Fock and coupling matrices with the KS counterparts. However, while the Wigner-Eckart theorem holds trivially in wave function approaches, it cannot naturally be fulfilled by approximate density functionals. For instance, the spin degeneracy condition (Ref. 10)

$$\left[K_{XC}^{\alpha\beta,\alpha\beta}\right]_{pq,rs} = \left[K_{XC}^{\beta\alpha,\beta\alpha}\right]_{pq,rs} = \left[K_{XC}^{T}\right]_{pq,rs}, \tag{11}$$

$$K_{XC}^{T} = \frac{1}{2}\left(K_{XC}^{\alpha\alpha,\alpha\alpha} - K_{XC}^{\alpha\alpha,\beta\beta} - K_{XC}^{\beta\beta,\alpha\alpha} + K_{XC}^{\beta\beta,\beta\beta}\right), \tag{12}$$

for a closed-shell system can only be fulfilled by a non-collinear parametrization[15] of the XC functional,[16–20] so as to retain the degeneracy of the three components of a triplet state. Yet, the SDC are case dependent. Consider again the doublet model shown in Fig. 1. Under the single pole

approximation (SPA) to UKS-based Tamm-Dancoff approximation (U-TDA), the excitation energy ω_{at}^{SC} for the spin-conserving OV($\alpha\alpha$) type of state $\Psi_t^a = |i\bar{i}a\rangle$ can be written as

$$\omega_{at}^{SC} = F_{aa}^{\alpha} - F_{tt}^{\alpha} + K_{at,at}^{\alpha\alpha,\alpha\alpha}. \tag{13}$$

On the other hand, the energy ω_{at}^{SF} for the state $\Psi_t^{\bar{a}} = |i\bar{i}\bar{a}\rangle$ due to the flip-up OV($\alpha\beta$) excitation reads

$$\omega_{at}^{SF} = F_{aa}^{\beta} - F_{tt}^{\alpha} + K_{at,at}^{\beta\alpha,\beta\alpha}. \tag{14}$$

The desired degeneracy $\omega_{at}^{SF} = \omega_{at}^{SC}$ implies the following SDC for this O-V excitation:

$$F_{aa}^{\beta} - F_{aa}^{\alpha} = K_{at,at}^{\alpha\alpha,\alpha\alpha} - K_{at,at}^{\beta\alpha,\beta\alpha}. \tag{15}$$

For a hybrid functional of the form

$$E_{XC} = c_X E_X^{HF} + (1 - c_X) E_{XC}^{DF}, \tag{16}$$

the left-hand side (LHS) of Eq. (15) reads

$$F_{aa}^{\beta} - F_{aa}^{\alpha} = c_X(at|ta) + (1 - c_X)\big(a\big|v_{XC}^{\beta} - v_{XC}^{\alpha}\big|a\big), \tag{17}$$

while the right-hand side (RHS) reads

$$\begin{aligned} &K_{at,at}^{\alpha\alpha,\alpha\alpha} - K_{at,at}^{\beta\alpha,\beta\alpha} \\ &\quad = (at|ta) + (1 - c_X)\big(at\big|f_{XC}^{\alpha\alpha,\alpha\alpha} - f_{XC}^{\beta\alpha,\beta\alpha}\big|ta\big). \end{aligned} \tag{18}$$

In terms of ROKS orbitals, we have $\rho^{\alpha} - \rho^{\beta} = |\phi_t|^2$, which leads to

$$\begin{aligned} \big(a\big|v_{XC}^{\beta} - v_{XC}^{\alpha}\big|a\big) &= -\left(at\left|\frac{v_{XC}^{\alpha} - v_{XC}^{\beta}}{\rho^{\alpha} - \rho^{\beta}}\right|ta\right) \\ &\triangleq -\big(at\big|f_{XC}^{\beta\alpha,\beta\alpha}\big|ta\big). \end{aligned} \tag{19}$$

Note that, while the first equality is specific to a doublet state, the second equality is just the definition of the noncollinear XC kernel for a general case.[16,19] Equation (17) can then be rewritten as

$$F_{aa}^{\beta} - F_{aa}^{\alpha} = c_X(at|ta) - (1 - c_X)\big(at\big|f_{XC}^{\beta\alpha,\beta\alpha}\big|ta\big). \tag{20}$$

In view of Eqs. (18) and (20), the difference $\delta\omega_{at}$ between the RHS and LHS of Eq. (15) becomes

$$\begin{aligned} \delta\omega_{at} &= \big(K_{at,at}^{\alpha\alpha,\alpha\alpha} - K_{at,at}^{\beta\alpha,\beta\alpha}\big) - \big(F_{aa}^{\beta} - F_{aa}^{\alpha}\big) \\ &= (1 - c_X)\big(at\big|f_H + f_{XC}^{\alpha\alpha,\alpha\alpha}\big|ta\big) = \omega_{at}^{SC} - \omega_{at}^{SF}, \end{aligned} \tag{21}$$

where $f_H = 1/|\vec{r}_1 - \vec{r}_2|$ represents the Coulomb kernel. Likewise, the SDC for the C-O type of excitations (i.e., $\Psi_{\bar{i}}^{\bar{t}} = -|it\bar{t}\rangle$ and $\Psi_i^{\bar{t}} = |\bar{i}t\bar{t}\rangle$) can be derived in the same way, viz.,

$$F_{ii}^{\beta} - F_{ii}^{\alpha} = K_{ti,ti}^{\beta\beta,\beta\beta} - K_{ti,ti}^{\beta\alpha,\beta\alpha}. \tag{22}$$

For the functional (16), the difference between the RHS and LHS of Eq. (22) reads

$$\begin{aligned} \delta\omega_{ti} &= \big(K_{ti,ti}^{\beta\beta,\beta\beta} - K_{ti,ti}^{\beta\alpha,\beta\alpha}\big) - \big(F_{ii}^{\beta} - F_{ii}^{\alpha}\big) \\ &= (1 - c_X)\big(it\big|f_H + f_{XC}^{\beta\beta,\beta\beta}\big|ti\big) = \omega_{ti}^{SC} - \omega_{ti}^{SF}. \end{aligned} \tag{23}$$

As expected, both $\delta\omega_{at}$ and $\delta\omega_{ti}$ vanish in the case of a pure HF exchange functional ($c_X = 1$). However, for other density functionals with $c_X \neq 1$, both $\delta\omega_{at}$ and $\delta\omega_{ti}$ are usually positive-valued, such that the spin-conserving excitation energies ω^{SC} are accordingly larger than the spin-flip ones ω^{SF}, thereby resulting in unphysical splittings of the doublets. In particular, pure density functionals ($c_X = 0$) give rise to the largest unphysical splittings. Note in passing that such splittings depend also on the nature of the excitations: They may be very large for local excitations where the involved orbitals have large overlaps, whereas they may be negligibly small for Rydberg or charge-transfer excitations where the orbitals have no appreciable overlaps. Such a tendency has already been observed by Wang and Ziegler[17] in calculations of doublet excited states using spin-flip U-TD-DFT in conjunction with the noncollinear local-density approximation (LDA) kernel.

The violation of the SDC (15) and (22) results in an ambiguity in evaluating the correction $\Delta\mathbf{A}$ (9) for the CV(1) type of excitations, which has been obtained through the Wigner-Eckart theorem and the assumption that different components of a multiplet are degenerate. For the considered model system, Eq. (9) reduces to

$$[\Delta\mathbf{A}]_{ai,ai}^{\mathrm{L}} = \big(F_{aa}^{\beta} - F_{aa}^{\alpha}\big) + \big(F_{ii}^{\beta} - F_{ii}^{\alpha}\big), \tag{24}$$

which is just the sum of the LHS of Eqs. (15) and (22). Yet, if the RHS of Eqs. (15) and (22) are to be employed, Eq. (9) will become

$$[\Delta\mathbf{A}]_{ai,ai}^{\mathrm{R}} = [\Delta\mathbf{A}]_{ai,ai}^{\mathrm{L}} + \delta\omega_{ai}, \quad \delta\omega_{ai} = \delta\omega_{at} + \delta\omega_{ti}, \tag{25}$$

which is usually larger than the value by Eq. (24). The peculiar point here is that the SDC violating term $\delta\omega_{ai}$ for the CV(1) type of excitations depends on the open-shell orbitals. In view of the formal relation $\omega^{SC} = \omega^{SF} + \delta\omega$ for the U-TD-DFT spin-conserving and spin-flip excitation energies for the C-O and O-V types of states (cf. Eqs. (21) and (23)), one may say that Eqs. (24) and (25) amount to using the respective spin-flip and spin-conserving excitations to evaluate the correction $\Delta\mathbf{A}$ (9) for spin-adapting the CV(1) type of excitations. The two agree with each other, only if the SDC (15) and (22) hold exactly. Given its simplicity, the analysis of this toy model paves the avenue for reformulating S-TD-DFT.

C. X-TD-DFT: S-TD-DFT amended with the exact spin degeneracy conditions

The very lesson from the previous analysis is that the exact SDC must properly be incorporated into S-TD-DFT. Since XC functionals satisfying the SDC are not yet available, we propose to simply combine the good of S-TD-DFT and S-RPA. That is, the correction term (9) is to be replaced with the corresponding RPA expression so as to guarantee the exact SDC. Specifically, the $\mathbf{A}$ and $\mathbf{B}$ matrices of spin-conserving S-TD-DFT (see Table I) are to be evaluated as

$$\mathbf{M}(S_i) = \mathbf{M}(S_i = \infty) + \Delta\mathbf{M}^{\mathrm{RPA}}, \quad \mathbf{M} = \mathbf{A}, \mathbf{B}, \tag{26}$$

$$\Delta\mathbf{M}^{\mathrm{RPA}} = \mathbf{M}^{\mathrm{RPA}}(S_i) - \mathbf{M}^{\mathrm{RPA}}(S_i = \infty). \tag{27}$$

The term $\mathbf{M}(S_i = \infty)$ represents the matrix obtained by taking the S_i to infinity in matrix elements of $\mathbf{M}$ and is actually

identical to the corresponding matrix of U-TD-DFT (Eq. (5)) when transformed to the spin-tensor basis.[21] The $\mathbf{M}^{\mathrm{RPA}}(S_i)$ matrix can also be read off Table I, just by regarding the various coupling terms $K^{\sigma\tau,\sigma'\tau'}$ as resulting from the HF expressions. As the RPA-type correction term $\Delta\mathbf{M}^{\mathrm{RPA}}$ satisfies the exact SDC by virtue of the Wigner-Eckart theorem, the ambiguity in evaluating the correction term (9) with approximate density functionals is now removed. Note that the same idea applies also to spin-flip S-TD-DFT but which is not considered here.

A few remarks are in order.

If the term $\Delta\mathbf{M}^{\mathrm{RPA}}$ is neglected, the resulting formalism is just spin-conserving U-TD-DFT but with ROKS orbitals. In this case, the XC kernel can only distinguish the $\alpha \rightarrow \alpha$ (i.e., OV($\alpha\alpha$) and CV($\alpha\alpha$)) from the $\beta \rightarrow \beta$ (i.e., CO($\beta\beta$) and CV($\beta\beta$)) types of transitions. The addition of the term $\Delta\mathbf{M}^{\mathrm{RPA}}$ brings more information into the XC kernel of U-TD-DFT, such that the distinctions between OV($\alpha\alpha$) and CV($\alpha\alpha$) and between CO($\beta\beta$) and CV($\beta\beta$) types of excitations are further accounted for. Consequently, all the four types of excitations can be treated more properly. Alternatively, Eq. (26) can be understood as follows. The spin-contaminated excited states produced by $\mathbf{M}(S_i = \infty)$ are broken-symmetry solutions as mixtures of different microstates of the same electronic configuration. The so-obtained excitation energies are, hence, averaged values of different spin multiplets, for which U-TD-DFT often offers a good estimate. The splittings of the microstates are then accounted for by the second term of Eq. (26) at the RPA level.

Another point to be addressed here is the double counting of correlation for the C-O and O-V types of excitations. Since the couplings between the C-O (or O-V) and C-V types of excitations have already been included in $\mathbf{M}(S_i = \infty)$, further mixing in the double excitations introduced for spin-adapting the CV(1) type of excitations may artificially lower the excitation energies for the C-O and O-V types of excitations. Therefore, such couplings should be removed from $\Delta\mathbf{M}^{\mathrm{RPA}}$. This can be achieved simply by setting the cross terms between the C-O (or O-V) and CV(1) types of excitations in $\Delta\mathbf{M}^{\mathrm{RPA}}$ to zero. The final nonzero matrix elements of $\Delta\mathbf{M}^{\mathrm{RPA}}$ are documented in Table II in both the spin-tensor and spin-orbital representations. They can all be constructed through the polarization ROHF matrix F^S

$$F^S_{pq} = \frac{1}{2}\left(F^{HF,\beta}_{pq} - F^{HF,\alpha}_{pq}\right) = \frac{1}{2}\sum_t (pt|tq). \tag{28}$$

Like $\mathbf{M}(S_i = \infty)$, the correction $\Delta\mathbf{M}^{\mathrm{RPA}}$ is manifestly invariant with respect to unitary transformations within the closed, open, and vacant orbital subspaces. This ansatz is to be dubbed as X-TD-DFT, to emphasize the incorporation of the exact SDC into S-TD-DFT, albeit with approximate XC functionals. Note that X-TD-DFT not only improves the accuracy (vide post) but also simplifies the calculation of the parent S-TD-DFT. As can be seen from Table I, the various coupling terms $K^{\sigma\tau,\sigma'\tau'}$ of S-TD-DFT are in the spin-tensor representation dependent on the type of orbitals so as to complicate the implementation and slow down the computation. In contrast, just like U-TD-DFT, X-TD-DFT involves a unified coupling term in the spin-orbital representation (see Eq. (6) for matrix $\mathbf{A}$, Eq. (7) for matrix $\mathbf{B}$, and Table II for $\Delta\mathbf{M}^{\mathrm{RPA}}$). The implementation of X-TD-DFT is, hence, truly simple: Only the one-electron term $\Delta\mathbf{M}^{\mathrm{RPA}}$ needs to be added into the U-TD-DFT routines working with ROKS orbitals.

Finally, it may be argued that the above removal of the double counting of correlation in $\Delta\mathbf{M}^{\mathrm{RPA}}$ is also meaningful for approximating the full S-RPA/S-TDA [viz., both $\mathbf{M}(S_i)$ and $\mathbf{M}(S_i = \infty)$ are RPA/TDA in Eq. (26)], leading to X-RPA/X-TDA. While the full S-TDA amounts to neglecting the couplings between the reference and the doubles of the CI Hamiltonian matrix in the basis composed of the reference, all the singles as well as only those doubles necessary for spin adaption, the so-obtained X-TDA is a more consistent approximation to the same CI problem by further decoupling part of the singles with those doubles. Again consider the doublet model in Fig. 1. At the S-TDA level, the full $\mathbf{A}^{\mathrm{TDA}}(S_i)$ allows the double excitation $\Psi^{\bar{t}a}_{\bar{i}t}$ to interact with both $\Psi^{\bar{t}}_{\bar{i}}$ (C-O type) and Ψ^{a}_{t} (O-V type) but not with the ground state Ψ_0. The latter interaction could appear only if Ψ_0 were also included in the configuration space. Since this is not the case, removing the cross term between $\Psi^{\bar{t}}_{\bar{i}}$ (or Ψ^{a}_{t}) and $\Psi^{\bar{t}a}_{\bar{i}t}$ in $\mathbf{A}^{\mathrm{TDA}}(S_i)$ should give rise to a more balanced treatment of both the ground and excited states. Note that while S-TDA is identical with the so-called extended single excitation configuration interaction[22] for doublet states, there is no direct counterpart for X-TDA.

TABLE II. Matrix elements of the S-RPA correction $\Delta\mathbf{A}$ (Eq. (27)) in the spin-tensor and spin-orbital representations. The corresponding $\Delta\mathbf{B}$ term is zero. The F^S matrix is defined in Eq (28). S_i: total spin of the reference.

Blocks	Matrix elements
	Spin-tensor basis
CV(0)-CV(0)	$[\Delta\mathbf{A}]_{ai,bj} = 0$
CV(0)-CV(1)	$[\Delta\mathbf{A}]_{ai,bj} = -(\sqrt{\frac{S_i+1}{S_i}} - 1)[\delta_{ij}F^S_{ab} - \delta_{ab}F^S_{ji}]$
CV(1)-CV(1)	$[\Delta\mathbf{A}]_{ai,bj} = \frac{1}{S_i}[\delta_{ij}F^S_{ab} + \delta_{ab}F^S_{ji}]$
	Spin-orbital basis
CV($\alpha\alpha$)-CV($\alpha\alpha$)	$[\Delta\mathbf{A}]_{ai,bj} = (1 - \sqrt{\frac{S_i+1}{S_i}} + \frac{1}{2S_i})\delta_{ij}F^S_{ab} + (-1 + \sqrt{\frac{S_i+1}{S_i}} + \frac{1}{2S_i})\delta_{ab}F^S_{ji}$
CV($\alpha\alpha$)-CV($\beta\beta$)	$[\Delta\mathbf{A}]_{ai,bj} = \frac{1}{2S_i}[\delta_{ij}F^S_{ab} + \delta_{ab}F^S_{ji}]$
CV($\beta\beta$)-CV($\beta\beta$)	$[\Delta\mathbf{A}]_{ai,bj} = (-1 + \sqrt{\frac{S_i+1}{S_i}} + \frac{1}{2S_i})\delta_{ij}F^S_{ab} + (1 - \sqrt{\frac{S_i+1}{S_i}} + \frac{1}{2S_i})\delta_{ab}F^S_{ji}$

III. COMPUTATIONAL DETAILS

In our previous work,[10] R-TD-DFT, U-TD-DFT, and S-TD-DFT were all implemented based on an existing TD-DFT module[18–20] in the BDF package.[23–26] The implementation only supports LDA, generalized gradient approximation (GGA), and statistical average of orbital model potentials[27] (SAOP) for ground states and the adiabatic local-density approximation (ALDA) of TD-DFT for excited states in conjunction with numerical or Slater type basis functions. To integrate the state-of-the-art density functionals, the DFT and TD-DFT modules are now rewritten in terms of Gaussian type of basis functions with the one- and two-electron integrals evaluated analytically, such that hybrid functionals and their collinear and noncollinear XC kernels can also be employed. The new TD-DFT module is capable of performing spin-conserving and spin-flip U-TD-DFT, R-TD-DFT, S-TD-DFT, and X-TD-DFT calculations for excited states with spin S_f equal to $S_i + 1$, S_i, or $S_i - 1$.

The low-lying doublet states of N_2^+ are to be taken as the touchstone for the performances of the various variants of TD-DFT and the effects of XC functionals. These include SVWN5,[28] SAOP,[27] BLYP,[29,30] LC-BLYP,[31] B3LYP,[32,33] CAM-B3LYP,[34] BHandHLYP,[29,30,32] and pure HF, which are featured by an increased amount of short-range HF exchange. As the considered states all arise from spin-conserving excitations, the collinear form of the XC kernels can be used. Problems associated with the noncollinear form of GGA kernels will be discussed elsewhere. The ROKS adopted here is defined through a unified coupling operator $\hat{R}$ (for details see Ref. 10). Different parametrizations of $\hat{R}$ are immaterial for functionals that are invariant with respect to unitary transformations within the closed, open, and vacant orbital subspaces but do affect the SAOP that depends explicitly on orbital energies. Nevertheless, it turns out that the SAOP constructed with the eigenvalues of $\hat{R}$ in place of the orbital energies is only weakly dependent on the parametrizations of the diagonal blocks of $\hat{R}$. For instance, the TD-DFT/SAOP energies for N_2^+ differ by only 0.02 eV for the parametrizations

$$\hat{R}_{XX} = \frac{1}{2}\left(F^{\alpha}_{XX} + F^{\beta}_{XX}\right), \quad X = C, O, V \tag{29}$$

and

$$\hat{R}_{XX} = F^{\alpha}_{XX}, \quad X = C, O, V. \tag{30}$$

The eigenvalues of the former parametrization[35] are usually very close to the averages of the UKS α and β spin orbital energies and are, hence, used throughout.

The TD-DFT results are to be compared with those by the MRCISD+Q (multi-reference configuration interaction with singles and doubles plus the Davidson correction) carried out with the Xi'an-CI module[36–38] interfaced into the BDF package. All the valence orbitals (i.e., $2\sigma_g 2\sigma_u 1\pi_u 3\sigma_g 1\pi_g 3\sigma_u$) are kept active in the SA-CASSCF (state-averaged complete active space self-consistent field) calculations. Compared with the previous MRCI calculations,[10] a different number of states are averaged here in the SA-CASSCF calculations. However, this results in some difference only of ~0.02 eV between the present and the previous MRCI vertical excitation energies. It turns out that the results by the aug-cc-pVTZ and aug-cc-pVQZ basis sets[39] are virtually identical for both TD-DFT and MRCI. Therefore, only the results by the aug-cc-pVTZ set will be reported.

IV. EXCITED STATES OF N_2^+: A SHOWCASE STUDY

The electronic configuration of N_2^+ is of the form $2\sigma_g^2 2\sigma_u^2 1\pi_u^4 3\sigma_g^1 1\pi_g^0 3\sigma_u^0$, with the orbitals ordered in ascending energy. Its low-lying doublet excited states arising from valence type of excitations are well below the first ionization potential. Therefore, the system represents a classic touchstone for the spin-contamination problem associated with open-shell TD-DFT, for the well-known failures of TD-DFT for Rydberg and charge-transfer excitations are out of the question. For this reason, the states of N_2^+ have been investigated by Ipatov *et al.*[9] using U-TD-DFT and also by the present authors[10] using U-TD-DFT, R-TD-DFT, and S-TD-DFT, all with the ALDA kernel. Apart from the new scheme of X-TD-DFT, the present work employs more refined functionals and, therefore, represents an extensive extension.

A. Vertical excitations

The vertical excitation energies for the low-lying doublet excited states of N_2^+ are first calculated at the experimental bond distance of 1.1164 Å.[40] Among the lowest ten doublet states, the $2^2\Pi_g$ and $3^2\Pi_g$ states, with respective energies of 9.91 and 11.02 eV, arise from double excitations according to the MRCI calculation.[10] They cannot be described at all by adiabatic TD-DFT and are, hence, not discussed here. The results for the other eight states by U-TD-DFT, S-TD-DFT, and X-TD-DFT in conjunction with various XC functionals are given in Table III, to be compared with the MRCI values. The corresponding TDA calculations are also carried out, with the results documented in Table IV. For a better illustration, the TD-DFT and TDA energies and their deviations from MRCI are further depicted in Figs. 2 and 3, respectively.

It is first seen from Fig. 3(a) that the $1^2\Pi_g$ state runs out of the trend: Its energy is overestimated by all the variants of TD-DFT and TDA, regardless of the chosen functionals. This is because the $1^2\Pi_g$ state has ~11% double excitations but that are missed by the adiabatic approximation. Another general feature is that, for the remaining states predominantly of single excitations, the TD-DFT excitation energies become progressively lowered as the mount of nonlocal exchange increases when going from BLYP through LC-BLYP, B3LYP, CAM-B3LYP, and BHandHLYP to pure HF. This stems mainly from the HF instability in the treatment of the ground state: Both the unrestricted Hartree-Fock (UHF) and ROHF wave functions are instable with respect to spatial symmetry breaking. Specifically, the mixing between the occupied $2\sigma_u\beta$ orbital and the virtual $3\sigma_g\beta$ orbital, as well as that between $1\pi_u$ with $1\pi_g$, breaks the inversion symmetry and can hence lower the UHF/ROHF energy. The ROHF solution is actually instable in the entire range of internuclear separations.[41] As a result, U-RPA, S-RPA, and X-RPA all give rise to imaginary excitation energies for $1^2\Sigma_u^+$ (see Table III). The

TABLE III. TD-DFT vertical excitation energies (in eV) of N_2^+ calculated at the distance of 1.1164 Å. Negative values indicate imaginary excitation energies. Statistical measures of the errors are relative to MRCI.

			U-TD-DFT							
State	Transition	MRCI	SVWN5	SAOP	BLYP	LC-BLYP	B3LYP	CAM-B3LYP	BHandHLYP	HF
$1^2\Pi_u$	$1\pi_u \rightarrow 3\sigma_g$	1.34	1.45	1.71	1.34	0.82	0.88	0.63	−0.25	1.30
$1^2\Sigma_u^+$	$2\sigma_u \rightarrow 3\sigma_g$	3.27	3.69	4.36	3.72	3.02	3.21	2.86	2.03	−3.92
$1^2\Pi_g$	$3\sigma_g \rightarrow 1\pi_g$	8.79	9.32	9.54	9.40	9.66	9.57	9.68	9.81	10.20
$2^2\Sigma_u^+$	$1\pi_u \rightarrow 1\pi_g$	9.33	7.38	7.49	6.95	6.69	6.48	6.32	5.52	2.89
$1^2\Sigma_u^-$	$1\pi_u \rightarrow 1\pi_g$	9.81	9.31	9.30	9.22	8.93	8.85	8.71	8.18	6.77
$1^2\Delta_u$	$1\pi_u \rightarrow 1\pi_g$	10.07	8.42	8.46	7.72	7.64	7.37	7.28	6.56	4.37
$2^2\Delta_u$	$1\pi_u \rightarrow 1\pi_g$	10.37	10.06	10.02	9.67	9.60	9.44	9.37	8.99	8.11
$2^2\Sigma_u^-$	$1\pi_u \rightarrow 1\pi_g$	11.09	9.55	9.50	9.48	9.14	9.13	8.97	8.51	7.32
$\bar{\Delta}$			−0.61	−0.46	−0.82	−1.07	−1.14	−1.28	−1.84	−3.38
Δ_{std}			0.98	1.14	1.18	1.19	1.28	1.30	1.52	3.04
$\bar{\Delta}_{\text{abs}}$			0.88	1.01	1.09	1.29	1.34	1.50	2.10	3.73
Δ_{max}			1.95	1.84	2.38	2.64	2.85	3.01	3.81	7.19
			S-TD-DFT							
State	Transition	MRCI	SVWN5	SAOP	BLYP	LC-BLYP	B3LYP	CAM-B3LYP	BHandHLYP	HF
$1^2\Pi_u$	$1\pi_u \rightarrow 3\sigma_g$	1.34	1.28	1.53	0.97	0.27	−0.18	−0.47	0.36	4.23
$1^2\Sigma_u^+$	$2\sigma_u \rightarrow 3\sigma_g$	3.27	3.48	4.15	3.48	2.67	2.80	2.37	0.45	−4.55
$1^2\Pi_g$	$3\sigma_g \rightarrow 1\pi_g$	8.79	9.24	9.51	9.25	9.46	9.32	9.40	9.29	8.95
$2^2\Sigma_u^+$	$1\pi_u \rightarrow 1\pi_g$	9.33	8.61	8.82	7.96	7.85	7.65	7.54	6.95	5.27
$1^2\Sigma_u^-$	$1\pi_u \rightarrow 1\pi_g$	9.81	9.40	9.35	9.31	9.01	8.94	8.80	8.30	6.98
$1^2\Delta_u$	$1\pi_u \rightarrow 1\pi_g$	10.07	9.56	9.66	8.65	8.71	8.41	8.37	7.78	6.42
$2^2\Delta_u$	$1\pi_u \rightarrow 1\pi_g$	10.37	10.07	10.03	9.66	9.60	9.44	9.38	9.00	8.14
$2^2\Sigma_u^-$	$1\pi_u \rightarrow 1\pi_g$	11.09	10.61	10.66	10.33	10.12	10.07	9.96	9.59	8.85
$\bar{\Delta}$			−0.23	−0.04	−0.56	−0.80	−0.95	−1.09	−1.54	−2.47
Δ_{std}			0.40	0.57	0.67	0.66	0.73	0.78	1.03	3.13
$\bar{\Delta}_{\text{abs}}$			0.39	0.49	0.72	0.97	1.08	1.24	1.67	3.24
Δ_{max}			0.72	0.88	1.42	1.49	1.68	1.80	2.82	7.82
			X-TD-DFT							
State	Transition	MRCI	SVWN5	SAOP	BLYP	LC-BLYP	B3LYP	CAM-B3LYP	BHandHLYP	HF
$1^2\Pi_u$	$1\pi_u \rightarrow 3\sigma_g$	1.34	1.42	1.66	1.27	0.74	0.79	0.54	−0.17	1.86
$1^2\Sigma_u^+$	$2\sigma_u \rightarrow 3\sigma_g$	3.27	3.74	4.39	3.74	3.03	3.23	2.87	2.02	−3.59
$1^2\Pi_g$	$3\sigma_g \rightarrow 1\pi_g$	8.79	9.28	9.56	9.33	9.56	9.44	9.54	9.56	9.60
$2^2\Sigma_u^+$	$1\pi_u \rightarrow 1\pi_g$	9.33	9.17	9.21	8.74	8.46	8.27	8.10	7.33	4.69
$1^2\Sigma_u^-$	$1\pi_u \rightarrow 1\pi_g$	9.81	9.39	9.35	9.31	9.00	8.95	8.80	8.30	6.98
$1^2\Delta_u$	$1\pi_u \rightarrow 1\pi_g$	10.07	9.93	9.88	9.40	9.30	9.06	8.97	8.31	6.49
$2^2\Delta_u$	$1\pi_u \rightarrow 1\pi_g$	10.37	10.33	10.29	9.78	9.69	9.53	9.46	9.05	8.14
$2^2\Sigma_u^-$	$1\pi_u \rightarrow 1\pi_g$	11.09	11.23	11.14	11.15	10.78	10.76	10.59	10.10	8.85
$\bar{\Delta}$			0.05	0.17	−0.17	−0.44	−0.51	−0.65	−1.20	−2.63
Δ_{std}			0.31	0.53	0.49	0.54	0.58	0.63	0.85	2.53
$\bar{\Delta}_{\text{abs}}$			0.24	0.39	0.44	0.63	0.67	0.84	1.39	2.96
Δ_{max}			0.49	1.12	0.67	0.87	1.06	1.23	2.01	6.86

instability problem is partly ameliorated by the hybrid functionals. However, the U-TD-DFT/BHandHLYP, S-TD-DFT/B3LYP, S-TD-DFT/CAM-B3LYP, and X-TD-DFT/BHandHLYP energies for the $1^2\Pi_u$ state are still imaginary. As can be seen from Fig. 3(b), the situation is much improved by the TDA variants, where the excitation manifold is decoupled from the ground-state instability. Nonetheless, the TDA results with the hybrid functionals are still much inferior to those by the pure density functionals (i.e., SVWN5, SAOP, and BLYP) which do not suffer from the instability problem at this geometry. The TD-DFT and TDA results with the pure functionals also do not differ much because the **B** term is rather small in these cases. Noticeably, SAOP overestimates the excitation energies of the first three states in all the TD-DFT variants.

The results are further analyzed in terms of the unsigned mean error $\bar{\Delta}$, the mean absolute error $\bar{\Delta}_{\text{abs}}$, the maximum absolute error Δ_{max} as well as the standard deviation Δ_{std} relative to MRCI, see Table III for TD-DFT and Table IV for TDA. Clearly, both S-TD-DFT and X-TD-DFT are superior over U-TD-DFT in conjunction with any density functional. Take B3LYP as an example; the $\bar{\Delta}_{\text{abs}}$ is 1.34 eV for U-TD-DFT, which is reduced to 1.08 eV by S-TD-DFT and further reduced to 0.67 eV by X-TD-DFT. The reduction of Δ_{std} is also significant: 1.28 eV for U-TD-DFT, 0.73 eV for S-TD-DFT, and 0.58 eV for X-TD-DFT, indicating more uniform

TABLE IV. TDA vertical excitation energies (in eV) of N_2^+ calculated at the distance of 1.1164 Å. For other explanations see Table III.

			U-TDA							
State	Transition	MRCI	SVWN5	SAOP	BLYP	LC-BLYP	B3LYP	CAM-B3LYP	BHandHLYP	HF
$1^2\Pi_u$	$1\pi_u \rightarrow 3\sigma_g$	1.34	1.53	1.77	1.45	0.96	1.06	0.86	0.55	−0.01
$1^2\Sigma_u^+$	$2\sigma_u \rightarrow 3\sigma_g$	3.27	4.10	4.69	4.09	3.46	3.67	3.41	3.12	2.15
$1^2\Pi_g$	$3\sigma_g \rightarrow 1\pi_g$	8.79	9.37	9.59	9.46	9.72	9.64	9.75	9.93	10.49
$2^2\Sigma_u^+$	$1\pi_u \rightarrow 1\pi_g$	9.33	7.69	7.76	7.35	7.20	7.10	7.00	6.63	5.65
$1^2\Sigma_u^-$	$1\pi_u \rightarrow 1\pi_g$	9.81	9.31	9.30	9.22	8.94	8.88	8.76	8.37	7.61
$1^2\Delta_u$	$1\pi_u \rightarrow 1\pi_g$	10.07	8.50	8.53	7.93	7.89	7.72	7.66	7.29	6.53
$2^2\Delta_u$	$1\pi_u \rightarrow 1\pi_g$	10.37	10.09	10.06	9.68	9.61	9.45	9.39	9.07	8.53
$2^2\Sigma_u^-$	$1\pi_u \rightarrow 1\pi_g$	11.09	9.55	9.50	9.48	9.16	9.15	9.02	8.69	8.07
$\bar{\Delta}$			−0.49	−0.36	−0.68	−0.89	−0.93	−1.03	−1.30	−1.88
Δ_{std}			1.00	1.17	1.16	1.14	1.20	1.21	1.36	1.73
$\bar{\Delta}_{\text{abs}}$			0.89	1.02	1.08	1.17	1.24	1.30	1.59	2.31
Δ_{max}			1.64	1.59	2.14	2.18	2.35	2.41	2.77	3.68
			S-TDA							
State	Transition	MRCI	SVWN5	SAOP	BLYP	LC-BLYP	B3LYP	CAM-B3LYP	BHandHLYP	HF
$1^2\Pi_u$	$1\pi_u \rightarrow 3\sigma_g$	1.34	1.40	1.63	1.24	0.76	0.80	0.58	0.13	−0.88
$1^2\Sigma_u^+$	$2\sigma_u \rightarrow 3\sigma_g$	3.27	3.99	4.57	3.96	3.32	3.49	3.22	2.80	1.47
$1^2\Pi_g$	$3\sigma_g \rightarrow 1\pi_g$	8.79	9.31	9.57	9.34	9.55	9.44	9.53	9.54	9.58
$2^2\Sigma_u^+$	$1\pi_u \rightarrow 1\pi_g$	9.33	8.94	9.09	8.37	8.34	8.23	8.17	7.91	7.40
$1^2\Sigma_u^-$	$1\pi_u \rightarrow 1\pi_g$	9.81	9.40	9.35	9.31	9.02	8.97	8.85	8.48	7.78
$1^2\Delta_u$	$1\pi_u \rightarrow 1\pi_g$	10.07	9.63	9.72	8.85	8.93	8.73	8.71	8.41	7.99
$2^2\Delta_u$	$1\pi_u \rightarrow 1\pi_g$	10.37	10.11	10.08	9.68	9.61	9.46	9.40	9.11	8.65
$2^2\Sigma_u^-$	$1\pi_u \rightarrow 1\pi_g$	11.09	10.61	10.66	10.33	10.13	10.10	10.00	9.75	9.50
$\bar{\Delta}$			−0.09	0.08	−0.37	−0.55	−0.61	−0.70	−0.99	−1.57
Δ_{std}			0.47	0.65	0.70	0.64	0.69	0.70	0.78	0.98
$\bar{\Delta}_{\text{abs}}$			0.41	0.52	0.68	0.75	0.82	0.88	1.18	1.77
Δ_{max}			0.72	1.30	1.22	1.14	1.34	1.36	1.66	2.22
			X-TDA							
State	Transition	MRCI	SVWN5	SAOP	BLYP	LC-BLYP	B3LYP	CAM-B3LYP	BHandHLYP	HF
$1^2\Pi_u$	$1\pi_u \rightarrow 3\sigma_g$	1.34	1.48	1.71	1.36	0.84	0.91	0.69	0.26	−0.69
$1^2\Sigma_u^+$	$2\sigma_u \rightarrow 3\sigma_g$	3.27	4.13	4.72	4.10	3.45	3.65	3.38	3.01	1.83
$1^2\Pi_g$	$3\sigma_g \rightarrow 1\pi_g$	8.79	9.33	9.61	9.38	9.62	9.51	9.61	9.68	9.91
$2^2\Sigma_u^+$	$1\pi_u \rightarrow 1\pi_g$	9.33	9.44	9.44	9.09	8.89	8.79	8.68	8.27	7.16
$1^2\Sigma_u^-$	$1\pi_u \rightarrow 1\pi_g$	9.81	9.39	9.35	9.31	9.02	8.97	8.85	8.49	7.78
$1^2\Delta_u$	$1\pi_u \rightarrow 1\pi_g$	10.07	9.97	9.92	9.50	9.42	9.24	9.18	8.79	8.01
$2^2\Delta_u$	$1\pi_u \rightarrow 1\pi_g$	10.37	10.40	10.35	9.87	9.78	9.65	9.58	9.26	8.65
$2^2\Sigma_u^-$	$1\pi_u \rightarrow 1\pi_g$	11.09	11.23	11.14	11.15	10.79	10.78	10.63	10.25	9.50
$\bar{\Delta}$			0.16	0.27	−0.04	−0.28	−0.32	−0.43	−0.76	−1.49
Δ_{std}			0.39	0.60	0.52	0.53	0.58	0.61	0.74	1.08
$\bar{\Delta}_{\text{abs}}$			0.29	0.43	0.42	0.53	0.60	0.67	0.98	1.77
Δ_{max}			0.86	1.45	0.83	0.82	0.83	0.95	1.32	2.17

descriptions of all the excited states by S-TD-DFT and especially by X-TD-DFT. Among all the TD-DFT and TDA variants and all the functionals, X-TD-DFT/SVWN5 performs the best for the eight low-lying excited states of N_2^+, which gives 0.05 eV for $\bar{\Delta}$, 0.31 eV for Δ_{std}, 0.24 eV for $\bar{\Delta}_{\text{abs}}$, and 0.49 eV for Δ_{max}. Such an accuracy is comparable to that of closed-shell TD-DFT for the lowest seven excited states of N_2 (−0.14 eV for $\bar{\Delta}$, 0.21 eV for Δ_{std}, 0.19 eV for $\bar{\Delta}_{\text{abs}}$, and 0.48 eV for Δ_{max} as evaluated from Table III of Ref. 10).

While the overall superiority of S-TD-DFT and X-TD-DFT over U-TD-DFT is obviously due to the proper spin-adaptation of the excited states, the improvement of X-TD-DFT over S-TD-DFT stems instead from the incorporation of the exact SDC and the removal of the double counting of correlation (see Sec. II C). Note first that, for the first two excited states dominated by the C-O type of excitations, S-TD-DFT with the functionals other than SVWN5 and SAOP tends to underestimate the excitation energies, whereas U-TD-DFT performs much better. This is a good indicator for the double counting of correlation. The C-O type of excitations are already spin-adapted[11] and can, hence, be well described by U-TD-DFT, particularly when the spin polarizations in the ground state are not dramatic. As such, further mixing the C-O type of excitations with the double excitations necessary for spin-adapting the CV(1) type of excitations, as done by S-TD-DFT, will deteriorate the already good U-TD-DFT

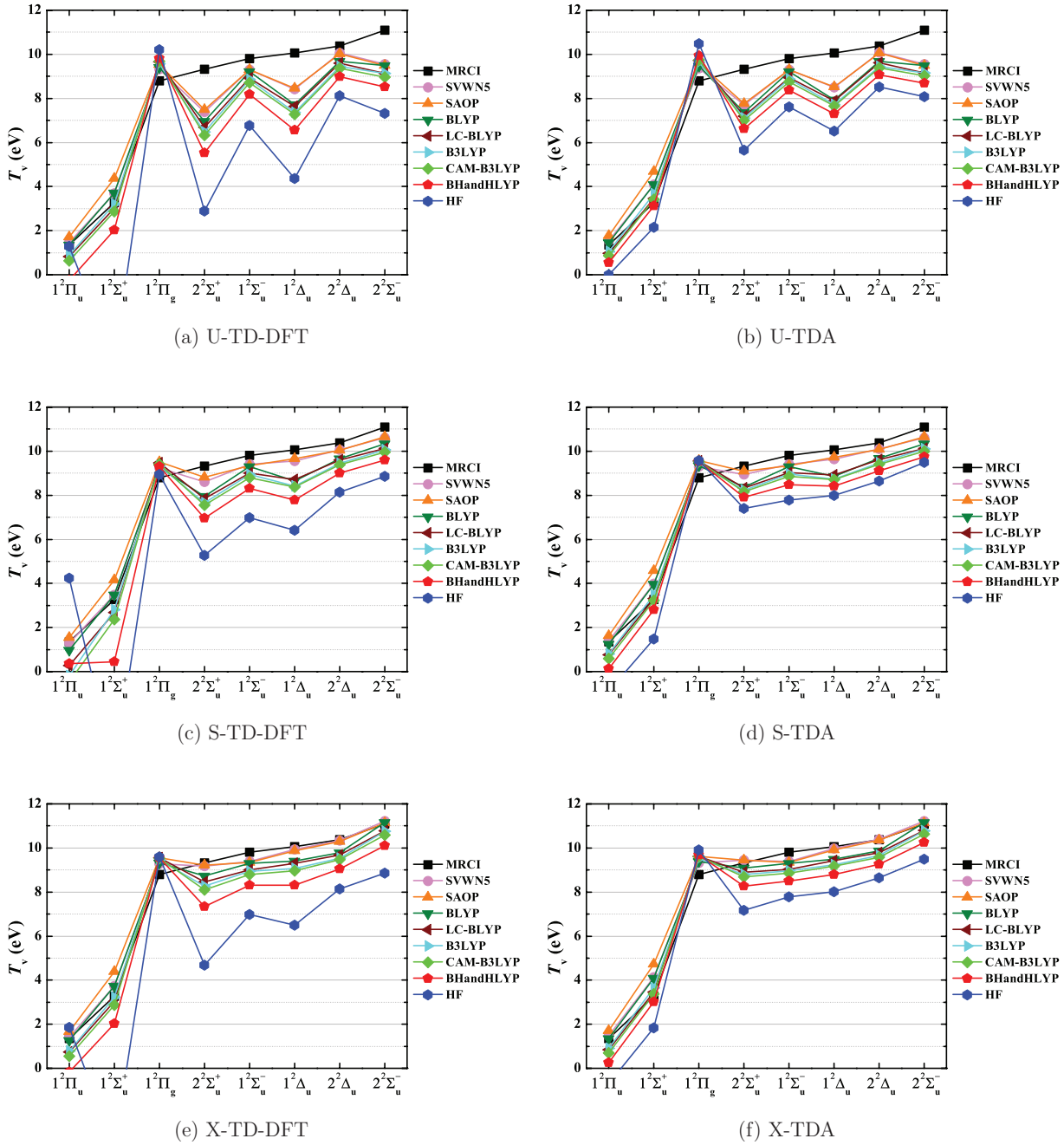

(a) U-TD-DFT (b) U-TDA

(c) S-TD-DFT (d) S-TDA

(e) X-TD-DFT (f) X-TDA

FIG. 2. (a)–(f) Vertical excitation energies (T_v in eV) of N_2^+ calculated at the distance of 1.1164 Å by MRCI, U-TD-DFT, S-TD-DFT, X-TD-DFT, and the TDA variants with various functionals.

results for these states. A similar finding was also observed in Ref. 42 where the attempt was to go beyond the adiabatic approximation by including two-particle/two-hole effects into the kernel. Such an artefact is removed deliberately by X-TD-DFT, whose results for these two states are indeed very close to the U-TD-DFT ones.

The improvement of X-TD-DFT over S-TD-DFT is also found for the fourth to eighth states born of the same configuration of $1\pi_u^3 3\sigma_g^1 1\pi_g^1$ arising from the $1\pi_u \rightarrow 1\pi_g$ transition. It is seen from Figs. 2(a) and 2(c) that, although S-TD-DFT improves significantly the U-TD-DFT energies for the $2^2\Sigma_u^+$, $1^2\Delta_u$, and $2^2\Sigma_u^-$ states, the S-TD-DFT energetic ordering for the fourth to eighth states is still incorrect for functionals from BLYP to pure HF, since the excitation energies for the $2^2\Sigma_u^+$ and $1^2\Delta_u$ states are still underestimated with these functionals. As can be seen from Fig. 2(e), the correct ordering is recovered by X-TD-DFT for all the functionals. Therefore, the S-RPA type of correction (Eq. (27)) for the CV(1) type of excitations provides indeed better splittings for the microstates of the same configuration, clearly reflecting the importance of the exact SDC.

After having discussed the overall features, we now discuss the individual states in more detail to gain deeper understandings on the S-RPA correction (27). The dominant components for every excited state obtained by U-TD-DFT, S-TD-DFT, and X-TD-DFT are listed in Table V. The

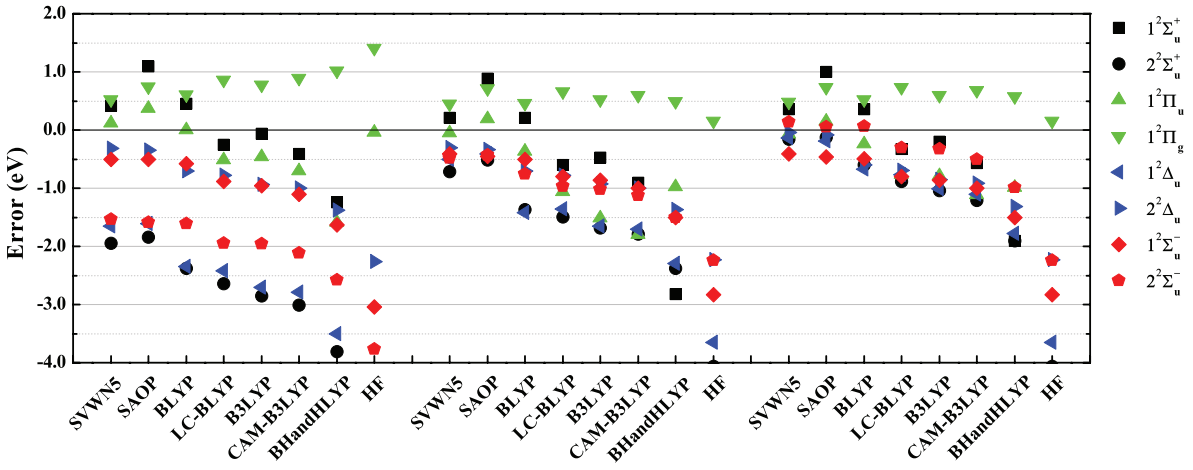

(a) U-TD-DFT, S-TD-DFT, and X-TD-DFT

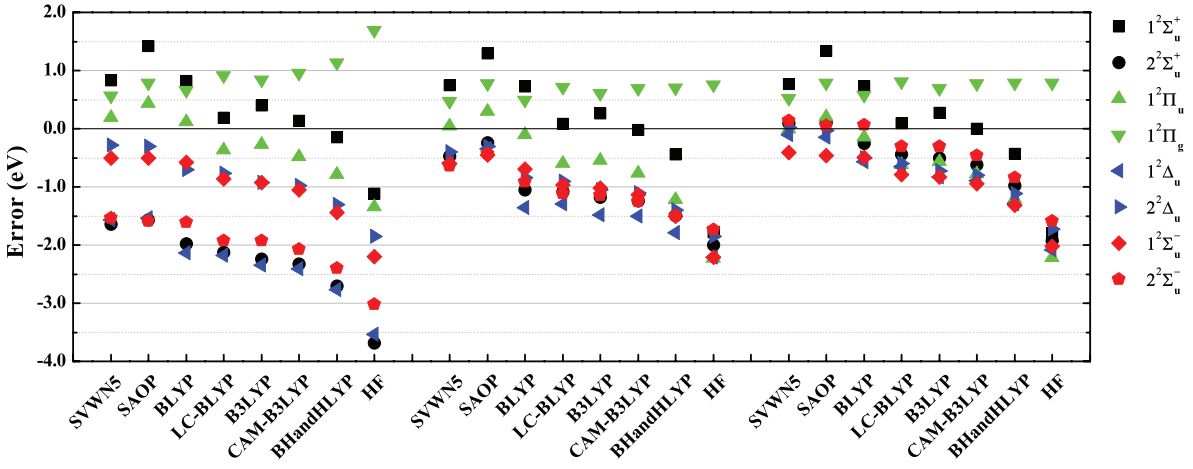

(b) U-TDA, S-TDA, and X-TDA

FIG. 3. (a) and (b) Deviations of TD-DFT and TDA from MRCI for vertical excitation energies (in eV) of N_2^+ calculated at the distance of 1.1164 Å.

TABLE V. Dominant transitions in the low-lying doublet states of N_2^+ calculated at the distance of 1.1164 Å. IPA: independent particle approximation; ω: vertical excitation energy; $\Delta\omega_1$=ω[S-TD-DFT]-ω[U-TD-DFT]; $\Delta\omega_2$=ω[X-TD-DFT]-ω[S-TD-DFT].

	U-TD-DFT				S-TD-DFT				X-TD-DFT			
State	ω ($\Delta\langle S^2\rangle$)	IPA		Transitions	ω ($\Delta\omega_1$)	IPA		Transitions	ω ($\Delta\omega_2$)	IPA		Transitions
$1^2\Pi_u$	1.45 (0.02)	1.51	98%	CO($\beta\beta$): $1\pi_u \rightarrow 3\sigma_g$	1.28 (−0.17)	1.47	97%	CO(0): $1\pi_u \rightarrow 3\sigma_g$	1.42 (0.14)	1.47	98%	CO(0): $1\pi_u \rightarrow 3\sigma_g$
$1^2\Sigma_u^+$	3.69 (0.14)	3.19	81%	CO($\beta\beta$): $2\sigma_u \rightarrow 3\sigma_g$	3.48 (−0.21)	3.19	78%	CO(0): $2\sigma_u \rightarrow 3\sigma_g$	3.74 (0.26)	3.19	84%	CO(0): $2\sigma_u \rightarrow 3\sigma_g$
		9.31	17%	CV($\alpha\alpha$): $1\pi_u \rightarrow 1\pi_g$		9.43	10%	CV(0): $1\pi_u \rightarrow 1\pi_g$		9.43	11%	CV(0): $1\pi_u \rightarrow 1\pi_g$
						10.59	10%	CV(1): $1\pi_u \rightarrow 1\pi_g$		11.23	3%	CV(1): $1\pi_u \rightarrow 1\pi_g$
$1^2\Pi_g$	9.32 (0.00)	9.12	99%	OV($\alpha\alpha$): $3\sigma_g \rightarrow 1\pi_g$	9.24 (−0.08)	9.08	99%	OV(0): $3\sigma_g \rightarrow 1\pi_g$	9.28 (0.04)	9.08	99%	OV(0): $3\sigma_g \rightarrow 1\pi_g$
$2^2\Sigma_u^+$	7.38 (1.98)	9.55	54%	CV($\beta\beta$): $1\pi_u \rightarrow 1\pi_g$	8.61 (1.23)	10.59	98%	CV(1): $1\pi_u \rightarrow 1\pi_g$	9.17 (0.56)	11.23	99%	CV(1): $1\pi_u \rightarrow 1\pi_g$
		9.31	45%	CV($\alpha\alpha$): $1\pi_u \rightarrow 1\pi_g$								
$1^2\Sigma_u^-$	9.31 (1.00)	9.31	100%	CV($\alpha\alpha$): $1\pi_u \rightarrow 1\pi_g$	9.40 (0.09)	9.43	98%	CV(0): $1\pi_u \rightarrow 1\pi_g$	9.39 (-0.01)	9.43	98%	CV(0): $1\pi_u \rightarrow 1\pi_g$
$1^2\Delta_u$	8.42 (2.00)	9.31	54%	CV($\alpha\alpha$): $1\pi_u \rightarrow 1\pi_g$	9.56 (1.13)	10.59	95%	CV(1): $1\pi_u \rightarrow 1\pi_g$	9.93 (0.37)	9.43	68%	CV(0): $1\pi_u \rightarrow 1\pi_g$
		9.55	46%	CV($\beta\beta$): $1\pi_u \rightarrow 1\pi_g$						11.23	32%	CV(1): $1\pi_u \rightarrow 1\pi_g$
$2^2\Delta_u$	10.06 (0.01)	9.55	55%	CV($\beta\beta$): $1\pi_u \rightarrow 1\pi_g$	10.07 (0.01)	9.43	96%	CV(0): $1\pi_u \rightarrow 1\pi_g$	10.33 (0.26)	11.23	74%	CV(1): $1\pi_u \rightarrow 1\pi_g$
		9.31	45%	CV($\alpha\alpha$): $1\pi_u \rightarrow 1\pi_g$						9.43	26%	CV(0): $1\pi_u \rightarrow 1\pi_g$
$2^2\Sigma_u^-$	9.55 (1.00)	9.55	100%	CV($\beta\beta$): $1\pi_u \rightarrow 1\pi_g$	10.61 (1.06)	10.59	98%	CV(1): $1\pi_u \rightarrow 1\pi_g$	11.23 (0.62)	11.23	98%	CV(1): $1\pi_u \rightarrow 1\pi_g$

TABLE VI. Analysis of the blueshift for the CV(1) type of transition ($1\pi_u \rightarrow 1\pi_g$).

	Spin-conserving, Eq. (13)			Spin-flip, Eq. (14)		Shift		
Transition	$\varepsilon_a^\alpha - \varepsilon_t^\alpha$	$(at\|ta)$	$(at\|f_{XC}^{\alpha\alpha,\alpha\alpha}\|ta)$	$\varepsilon_a^\beta - \varepsilon_t^\alpha$	$(at\|f_{XC}^{\beta\alpha,\beta\alpha}\|ta)$	LHS of Eq. (15)	RHS of Eq. (15)	Eq. (27)
OV: $3\sigma_g \rightarrow 1\pi_g$	9.12	1.09	−0.74	9.82	−0.68	0.70	1.03	1.09
Transition	$\varepsilon_t^\beta - \varepsilon_i^\beta$	$(ti\|it)$	$(ti\|f_{XC}^{\beta\beta,\beta\beta}\|it)$	$\varepsilon_t^\beta - \varepsilon_i^\alpha$	$(ti\|f_{XC}^{\beta\alpha,\beta\alpha}\|it)$	LHS of Eq. (22)	RHS of Eq. (22)	Eq. (27)
CO: $1\pi_u \rightarrow 3\sigma_g$	1.51	0.72	−0.59	1.98	−0.48	0.47	0.61	0.72
Total shift						1.17	1.64	1.81

excitation energies by the independent particle approximation (IPA) are also shown for comparison. Note that, in the case of X-TD-DFT, the diagonal terms of the S-RPA correction (27) are also ascribed to the IPA. As the differences between the U-TD-DFT and S-TD-DFT results have already been scrutinized before,[10] we focus here on the comparison between S-TD-DFT and X-TD-DFT. It is first seen that the S-TD-DFT energies for the states dominated by the CV(1) type of excitations are blueshifted by X-TD-DFT. The amounts of the blueshifts, i.e., 0.56, 0.62, 0.37, and 0.26 eV for the respective $2^2\Sigma_u^+$, $2^2\Sigma_u^-$, $1^2\Delta_u$, and $2^2\Delta_u$ states, are well correlated with the difference (0.64 eV) between the X-TD-DFT (11.23 eV) and S-TD-DFT (10.59 eV) IPA values for the CV(1) $1\pi_u \rightarrow 1\pi_g$ transition. It is just that the sum (0.63 eV) of the shifts for $1^2\Delta_u$ and $2^2\Delta_u$ should be taken as a whole, as they are paired from linear combinations of the S-TD-DFT $1^2\Delta_u$ and $2^2\Delta_u$ states. Noticeably, the energetically higher $2^2\Delta_u$ state is in S-TD-DFT composed purely of the CV(0) instead of the CV(1) transition, although the former has a much smaller IPA energy (9.43 vs. 10.59 eV). This results from the coupling terms, which are negative for CV(1) but become positive for CV(0) due to the additional Coulomb term, thereby reversing the ordering of the CV(0) and CV(1) transitions constituting the $1^2\Delta_u$ and $2^2\Delta_u$ states. Indeed, the S-TD-DFT/SVWN5 energy (10.07 eV) for $2^2\Delta_u$ is in line with the MRCI (10.07 eV) and X-TD-DFT (9.93 eV) values for $1^2\Delta_u$ (see Table IV). If the additional blueshift of 0.64 eV by the correction term (27) is simply added to the S-TD-DFT energy (9.56 eV) for $1^2\Delta_u$, a value of 10.20 eV is to be obtained, which is close to the X-TD-DFT (10.33 eV) and MRCI (10.37 eV) values for $2^2\Delta_u$. As the two states are of the same symmetry, the incorrect ordering by S-TD-DFT (and U-TD-DFT) cannot readily be identified. In contrast, X-TD-DFT does predict the expected ordering: $1^2\Delta_u$ and $2^2\Delta_u$ are dominated, respectively, by the CV(0) and CV(1) transitions, in line with the MRCI prediction. Therefore, X-TD-DFT not only improves the energies but also the wave functions of S-TD-DFT.

To further analyze the overall shift of 0.64 eV introduced by the S-RPA correction (27), all the relevant quantities discussed in Sec. II B are calculated with the UKS/SVWN5 reference for the $3\sigma_g \rightarrow 1\pi_g$ and $1\pi_u \rightarrow 3\sigma_g$ transitions (see Table VI). As shown before,[10] the SPA energies for the OV($\alpha\beta$) and CO($\alpha\beta$) flip-down excitations should be equal to the IPA energies of the corresponding spin-conserving transitions. This is indeed the case here: The SPA energies for the $3\sigma_g\alpha \rightarrow 1\pi_g\beta$ (9.14 eV) and $1\pi_u\alpha \rightarrow 3\sigma_g\beta$ (1.50 eV) transitions are very close to the orbital energy differences between $1\pi_g\alpha$ and $3\sigma_g\alpha$ (9.12 eV) and between $3\sigma_g\beta$ and $1\pi_u\beta$ (1.51 eV). The tiny discrepancies in-between arise from the use of different orbitals for different spin. The blueshift of S-TD-DFT over U-TD-DFT as calculated by Eq. (24) or the sum of the LHS of Eqs. (15) and (22) is 1.17 eV, which is very close to the actual values $\Delta\omega_1$ for the CV(1) type of excitations (see Table V). This is different from the value of 1.64 eV by Eq. (25) or the sum of the RHS of Eqs. (15) and (22), reflecting the violation of the SDC. The S-RPA term (27) is calculated to be 1.81 eV, which explains nicely the 0.64 eV (=1.81 − 1.17) shift of X-TD-DFT over S-TD-DFT. At this moment, it is worth mentioning that the TD-DFT sum method[43] (see also Ref. 11) combined with the present correction (27) for spin degeneracy allows us to retrieve the excitation energies for pure spin states from the spin-conserving and spin-flip U-TD-DFT results. However, the procedure is rather involved and is applicable only to a pair of states arising from a pure C-V transition. In contrast, the present X-TD-DFT amounts to integrating the procedure into a single equation, from which all the states of correct spin symmetry can be obtained in one time.

TABLE VII. Vertical excitation energies (in eV) for the high-lying states of N_2^+ calculated at the distance of 1.1164 Å. The states are ordered according to the X-TD-DFT/SAOP energies. The $\Delta\langle S^2\rangle$ values for U-TD-DFT are in parentheses. V: valence; R: Rydberg.

		SVWN5/aug-cc-pVTZ			SAOP/aug-cc-pVTZ			
State	Transition	U-TD-DFT	S-TD-DFT	X-TD-DFT	U-TD-DFT	S-TD-DFT	X-TD-DFT	MRCI
$2^2\Pi_u$	V: $2\sigma_u \rightarrow 1\pi_g$	10.52 (1.96)	12.23	12.67	10.99 (1.96)	12.80	13.10	12.55 (74% $2\sigma_u \rightarrow 1\pi_g$)
$3^2\Sigma_u^+$	V: $1\pi_u \rightarrow 1\pi_g$	16.09 (0.00)	16.05	16.01	16.16 (0.00)	16.10	16.07	16.15 (88% $1\pi_u \rightarrow 1\pi_g$)
$3^2\Pi_u$	R: $1\pi_u \rightarrow 4\sigma_g$	13.77 (0.05)	14.10	17.73	14.22 (0.06)	14.72	17.97	16.14 (59% $2\sigma_u \rightarrow 1\pi_g$, 24% $1\pi_u 3\sigma_g \rightarrow 1\pi_g^2$)
$2^2\Sigma_g^+$	R: $3\sigma_g \rightarrow 4\sigma_g$	17.78 (0.02)	17.71	17.74	18.39 (0.02)	18.28	18.32	12.94 (66% $2\sigma_u 1\pi_u \rightarrow 3\sigma_g 1\pi_g$, 10% $2\sigma_g \rightarrow 3\sigma_g$)

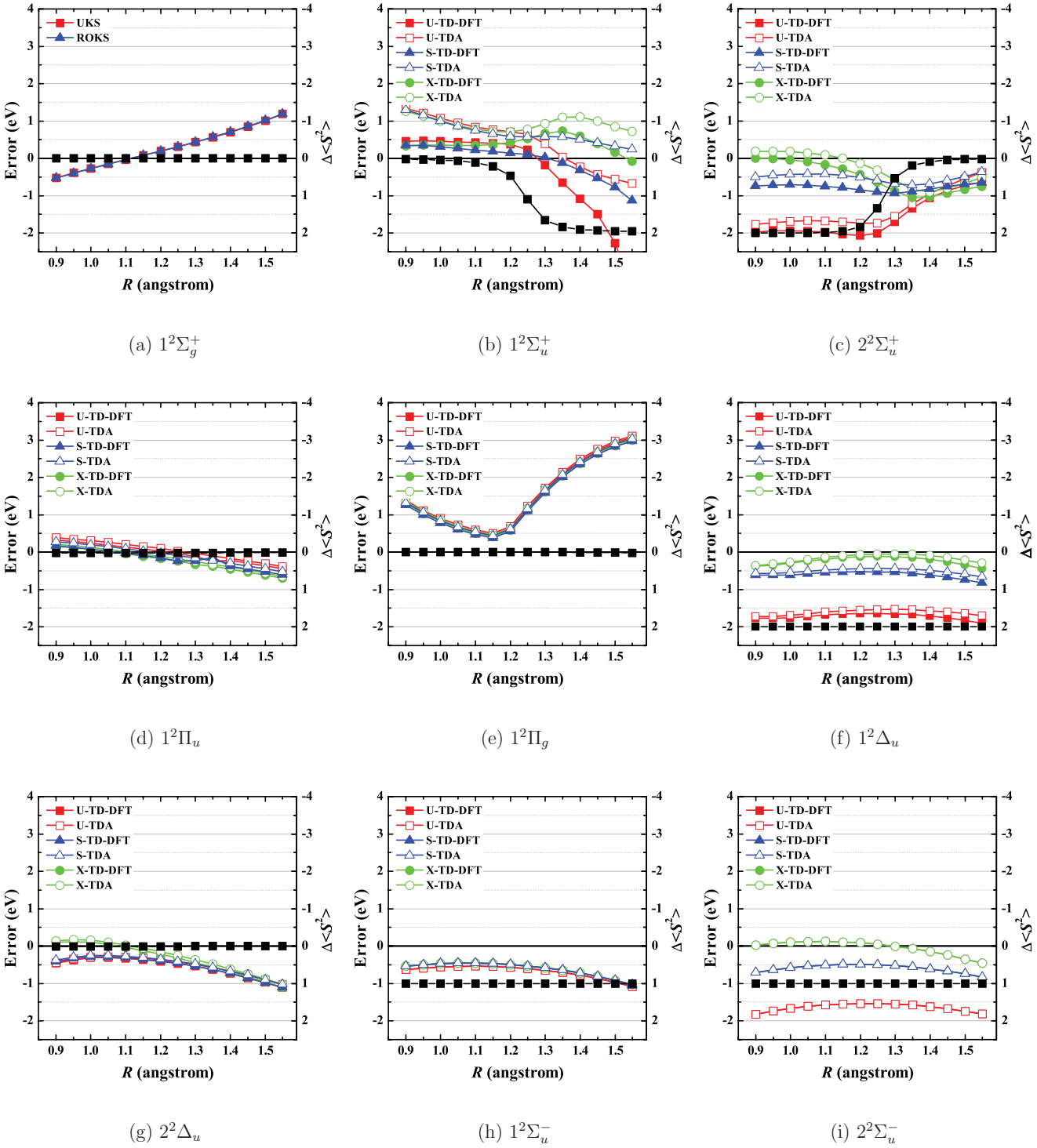

FIG. 4. Deviations of TD-DFT/SVWN5 and TDA/SVWN5 from MRCI for potential energy curves of the ground and excited states of N_2^+. The TD-DFT and TDA curves coincide for the $1^2\Sigma_u^-$ and $2^2\Sigma_u^-$ states. The $\Delta\langle S^2\rangle$ values are indicated by black squares. (a) UKS and ROKS ground states. (b)–(i) Doublet excited states.

B. Potential energy curves

To further examine the performances of the various variants of TD-DFT, the potential energy curves of the doublet states of N_2^+ are also calculated, to be compared with those from the TDA variants and MRCI. The calculations are performed for interatomic distances R between 0.90 and 1.55 Å with an interval of 0.05 Å. For brevity, only the deviations of TD-DFT/SVWN5 and TDA/SVWN5 from MRCI are depicted in Fig. 4, with the deviations decomposed into the ground and excited state components

$$\Delta E_I = \Delta E_0 + \Delta\omega_I, \tag{31}$$

$$\Delta E_0 = E_0(\mathrm{DFT}) - E_0(\mathrm{MRCI}), \quad (32)$$

$$\Delta\omega_I = \omega_I(\mathrm{TDDFT}) - [E_I(\mathrm{MRCI}) - E_0(\mathrm{MRCI})]. \quad (33)$$

The ΔE_0 for the ground state is shown in Fig. 4(a), while the $\Delta\omega_I$ for the excited states are shown in Figs. 4(b)–4(i). To diagnose the spin contamination in the UKS and U-TD-DFT results, the deviation $\Delta\langle S^2\rangle$ of the expectation value of the square of the total spin angular momentum S^2 from the exact value of zero is also shown in the same figure for each state. It is first seen that the extent of spin contamination in the $1^2\Sigma_u^+$ and $2^2\Sigma_u^+$ states changes dramatically as the interatomic distance increases: The $\Delta\langle S^2\rangle$ value for $1^2\Sigma_u^+$ is approximately zero at shorter distances, approaches to one around 1.25 Å, and then becomes two afterwards, whereas the reverse is true for $2^2\Sigma_u^+$. This indicates the interchange in the characters of the two states before and after 1.25 Å, characteristic of the avoided crossing around 1.25 Å. In contrast, the $\Delta\langle S^2\rangle$ values are approximately zero for $1^2\Pi_u$, $1^2\Pi_g$, and $2^2\Delta_u$, one for $1^2\Sigma_u^-$ and $2^2\Sigma_u^-$, and two for $1^2\Delta_u$ throughout the internuclear separations. Clearly, all the various variants of TD-DFT perform rather similarly for the states with little spin contamination, whereas both S-TD-DFT and X-TD-DFT outperform U-TD-DFT for those heavily spin-contaminated states. Especially, X-TD-DFT further improves S-TD-DFT for those states with contributions from the CV(1) type of excitations, e.g., the $1^2\Sigma_u^+$ state at $R > 1.25$ Å, the $2^2\Sigma_u^+$ state at $R < 1.25$ Å, as well as the $1^2\Delta_u$ and $2^2\Sigma_u^-$ states throughout the internuclear separations. Therefore, it can be concluded that X-TD-DFT outperforms S-TD-DFT (and U-TD-DFT) for the whole geometry, provided that the ROKS remains a valid approximation for the ground state.

C. Even higher states

Having scrutinized the eight low-lying excited sates of N_2^+, it remains to see whether even higher states can also be described correctly. For this purpose, the vertical excitation energies for the next four states of N_2^+ are calculated by U-TD-DFT, S-TD-DFT, and X-TD-DFT with SVWN5 and SAOP (see Table VII). The MRCI calculation is based on the SA-CASSCF with $4\sigma_g$ also in the active space. It is seen that, due to spin contamination, U-TD-DFT underestimates severely the energy of $2^2\Pi_u$, which is blueshifted by 1.71 eV by S-TD-DF and further by 0.44 eV by X-TD-DFT, leading finally to a good agreement with the MRCI value. Being free of spin contamination, the TD-DFT energies for the $3^2\Sigma_u^+$ state are all very close to each other and also to the MRCI value. However, the $3^2\Pi_u$ and $2^2\Sigma_g^+$ states are predicted by TD-DFT as Rydberg states, very different from the MRCI prediction, where $3^2\Pi_u$ is a heavy mixture of single and double excitations, while $2^2\Sigma_g^+$ is even dominated by double excitations. Therefore, these two states cannot be correctly handled by adiabatic TD-DFT. The situation with still higher states is rather similar and will not further be discussed. In sum, under the adiabatic approximation, TD-DFT is able to describe correctly only ten doublet states of N_2^+ dominated by single excitations.

V. CONCLUSIONS AND OUTLOOK

It has been shown that it is absolutely essential to impose the exact spin degeneracy conditions in open-shell TD-DFT in conjunction with approximate functionals. The resulting formalism, X-TD-DFT, is not only more accurate but also simpler than the parent S-TD-DFT. In essence, X-TD-DFT combines the good of S-TD-DFT and S-RPA: S-TD-DFT is grossly good for excitation energies while S-RPA is grossly good for multiplet splittings. The removal of the double counting of correlation turns out to be also important to avoid overcorrection of the already spin-adapted transitions. As X-TD-DFT is just a simple correction to U-TD-DFT, the implementation can simply be done by adding the one-electron increment to the U-TD-DFT routines running with ROKS orbitals. Note that the same idea can also be applied to the spatial symmetry contamination problem by combining the normal TD-DFT with a space-adapted RPA correction. As X-TD-DFT is invariant with unitary transformations within the closed, open, and vacant orbital subspaces, it can readily be combined with the recently proposed linear scaling TD-DFT in terms of localized molecular orbitals.[44]

As demonstrated here for the first time, the accuracy of open-shell and closed-shell TD-DFT can be made comparable. As a side caveat, hybrid functionals should be used with caution as they often run into the HF instability problem in open-shell systems. These findings apply also to a large test set of systems, not documented here though. Therefore, X-TD-DFT can be recommended as a valuable tool for excited states of high spin open-shell systems.

ACKNOWLEDGMENTS

The research of this work was supported by grants from the National Natural Science Foundation of China (Project No. 21033001).

[1] J. Stanton and R. J. Bartlett, J. Chem. Phys. **98**, 7029 (1993).
[2] D. C. Comeau and R. J. Bartlett, Chem. Phys. Lett. **207**, 414 (1993).
[3] E. Runge and E. K. U. Gross, Phys. Rev. Lett. **52**, 997 (1984).
[4] M. Petersilka, U. Gossmann, and E. K. U. Gross, Phys. Rev. Lett. **76**, 1212 (1996).
[5] M. E. Casida, in *Recent Advances in Density Functional Methods*, edited by D. P. Chang (World Scientific, Singapore, 1995), Vol. 1.
[6] P. G. Szalay and J. Gauss, J. Chem. Phys. **112**, 4027 (2000).
[7] R. C. Fortenberry, R. A. King, J. F. Stanton, and T. D. Crawford, J. Chem. Phys. **132**, 144303 (2010).
[8] M. E. Casida, J. Chem. Phys. **122**, 054111 (2005).
[9] A. Ipatov, F. Cordova, L. J. Doriol, and M. E. Casida, J. Mol. Struct.: THEOCHEM **914**, 60 (2009).
[10] Z. Li, W. Liu, Y. Zhang, and B. Suo, J. Chem. Phys. **134**, 134101 (2011).
[11] Z. Li and W. Liu, J. Chem. Phys. **133**, 064106 (2010).
[12] O. Vahtras and Z. Rinkevicius, J. Chem. Phys. **126**, 114101 (2007).
[13] D. Jacquemin, V. Wathelet, E. A. Perpète, and C. Adamo, J. Chem. Theory Comput. **5**, 2420 (2009).
[14] J. P. Perdew and K. Schmidt, in *Density Functional Theory and Its Applications to Materials*, AIP Conference Proceedings Vol. 577, edited by V. E. Van Doren, C. Van Alsenoy, and P. Geerlings (American Institute of Physics, Melville, NY, 2001), pp. 1–20.
[15] F. Wang and W. Liu, J. Chin. Chem. Soc. (Taipei) **50**, 597 (2003).
[16] F. Wang and T. Ziegler, J. Chem. Phys. **121**, 12191 (2004).
[17] F. Wang and T. Ziegler, J. Chem. Phys. **122**, 074109 (2005).
[18] J. Gao, W. Liu, B. Song, and C. Liu, J. Chem. Phys. **121**, 6658 (2004).

[19]J. Gao, W. Zou, W. Liu, Y. Xiao, D. Peng, B. Song, and C. Liu, J. Chem. Phys. **123**, 054102 (2005).
[20]D. Peng, W. Zou, and W. Liu, J. Chem. Phys. **123**, 144101 (2005).
[21]Actually, compared with U-TD-DFT, an additional term $\delta_{uv} F_{bi}^{\beta}$ in $[\mathbf{B}]_{ui,bv}$ (cf. Table I) still survives after setting S_i to infinity if ROKS orbitals are used. However, this term is negligibly small.
[22]D. Maurice and M. Head-Gordon, J. Phys. Chem. **100**, 6131 (1996).
[23]W. Liu, G. Hong, D. Dai, L. Li, and M. Dolg, Theor. Chem. Acc. **96**, 75 (1997).
[24]W. Liu, F. Wang, and L. Li, J. Theor. Comput. Chem. **2**, 257 (2003).
[25]W. Liu, F. Wang, and L. Li, in *Recent Advances in Relativistic Molecular Theory*, Recent Advances in Computational Chemistry Vol. 5, edited by K. Hirao and Y. Ishikawa (World Scientific, Singapore, 2004), p. 257.
[26]W. Liu, F. Wang, and L. Li, in *Encyclopedia of Computational Chemistry (electronic edition)*, edited by P. von Ragué Schleyer, N. L. Allinger, T. Clark, J. Gasteiger, P. A. Kollman, H. F. Schaefer III, and P. R. Schreiner (Wiley, Chichester, 2004).
[27]P. R. T. Schipper, O. V. Gritsenko, S. J. A. van Gisbergen, and E. J. Baerends, J. Chem. Phys. **112**, 1344 (2000).
[28]S. H. Vosko, L. Wilk, and M. Nusair, Can. J. Phys. **58**, 1200 (1980).
[29]A. D. Becke, Phys. Rev. A **38**, 3098 (1988).
[30]C. Lee, W. Yang, and R. G. Parr, Phys. Rev. B **37**, 785 (1988).
[31]H. Iikura, T. Tsuneda, T. Yanai, and K. Hirao, J. Chem. Phys. **115**, 3540 (2001).
[32]A. D. Becke, J. Chem. Phys. **98**, 5648 (1993).
[33]P. J. Stephens, F. J. Devlin, C. F. Chabalowski, and M. J. Frisch, J. Phys. Chem. **98**, 11623 (1994).
[34]T. Yanai, D. P. Tew, and N. C. Handy, Chem. Phys. Lett. **393**, 51 (2004).
[35]M. F. Guest and V. R. Saunders, Mol. Phys. **28**, 819 (1974).
[36]Y. Wang, G. Zhai, B. Suo, Z. Gan, and Z. Wen, Chem. Phys. Lett. **375**, 134 (2003).
[37]Y. Wang, H. Han, G. Zhai, B. Suo, and Z. Wen, Sci. China, Ser. B: Chem. **47**, 276 (2004).
[38]B. Suo, G. Zhai, Y. Wang, Z. Wen, X. Hu, and L. Li, J. Comput. Chem. **26**, 88 (2005).
[39]T. H. Dunning, Jr., J. Chem. Phys. **90**, 1007 (1989).
[40]K. P. Huber and G. Herzberg, *Molecular Spectra and Molecular Structure*, Constants of Diatomic Molecules Vol. IV (Van Nostrand, New York, 1979).
[41]X. Li and J. Paldus, Phys. Chem. Chem. Phys. **11**, 5281 (2009).
[42]M. Huix-Rotllant, A. Ipatov, A. Rubio, and M. E. Casida, "Assessment of dressed time-dependent density-functional theory for the low-lying valence states of 28 organic chromophores," Chem. Phys. (in press).
[43]M. Seth and T. Ziegler, J. Chem. Phys. **123**, 144105 (2005).
[44]F. Wu, W. Liu, Y. Zhang, and Z. Li, J. Chem. Theory Comput. **7**, 3643 (2011).